Earth, Planets and Space

FULL PAPER Open Access

Middle Miocene forearc alkaline magmatism in Amami-Oshima Island, central Ryukyu Arc: implications for paleoreconstruction of Shikoku Basin

Ginta Motohashi[1,2,6*], Osamu Ishizuka[2], Hirokuni Oda[2], Takashi Sano[3], Shun Sekimoto[4] and Kohtaro Ujiie[5]

Abstract

During the middle Miocene, forearc alkaline magmatism occurred in the Outer Zone of Southwest Japan and the northern Ryukyu Arc, resulting in the formation of forearc alkaline basaltic rocks with ocean island basalt (OIB)-like chemical signatures. In contrast, subduction-related magmatism was present in the central Ryukyu Arc. However, the southwestern margin of the forearc alkaline magmatism was poorly constrained in the Ryukyu Arc. We examined two basaltic dikes in the Chichibu accretionary complex of Amami-Oshima Island, the central Ryukyu Arc. The dikes cut massive basalt, reddish chert, varicolored shale, and grey chert. The chemical compositions of basaltic dikes are characterized by the enrichment of incompatible trace elements, possibly representing a low degree of partial melting from a deep mantle source. $^{40}Ar/^{39}Ar$ dating analyses indicate that the basaltic dikes yield ages of 16.37 ± 0.14 Ma and 16.51 ± 0.10 Ma. The paleomagnetic analyses on stepwise thermal demagnetizations allowed extracting the direction of stable magnetizations with unblocking temperatures of 450–575 °C for the two dikes [(Dec, Inc) = (138.1°, − 13.3°), (124.0°, − 24.9°)]. The magnetization could be primary, acquired either as part of a secular variation or a geomagnetic excursion during reversed polarity chron/subchron. The $^{40}Ar/^{39}Ar$ ages and paleomagnetic directions within the error range imply that they intruded almost simultaneously during C5Cn.2r (16.532–16.434 Ma). The age and trace element patterns of the basaltic dikes are comparable to those of Miocene alkaline basaltic rocks, which resulted from forearc alkaline magmatism during the initial subduction of the young and warm Shikoku Basin. The discovery of alkaline basaltic dikes on Amami-Oshima Island suggests that the distribution of middle Miocene forearc alkaline magmatism may extend to the central Ryukyu Arc. Hence, the northern end of the Kyushu-Palau Ridge (i.e., southern end of Shikoku Basin) could have been located south of Amami-Oshima Island around 16.5–16.4 Ma, then moved eastward to the current location.

Keywords Miocene, Ryukyu Arc, Amami-Oshima Island, Basaltic dike, Alkaline basalt, OIB, Forearc magmatism

*Correspondence:
Ginta Motohashi
motohashi.ginta.md@alumni.tsukuba.ac.jp
Full list of author information is available at the end of the article

Graphical Abstract

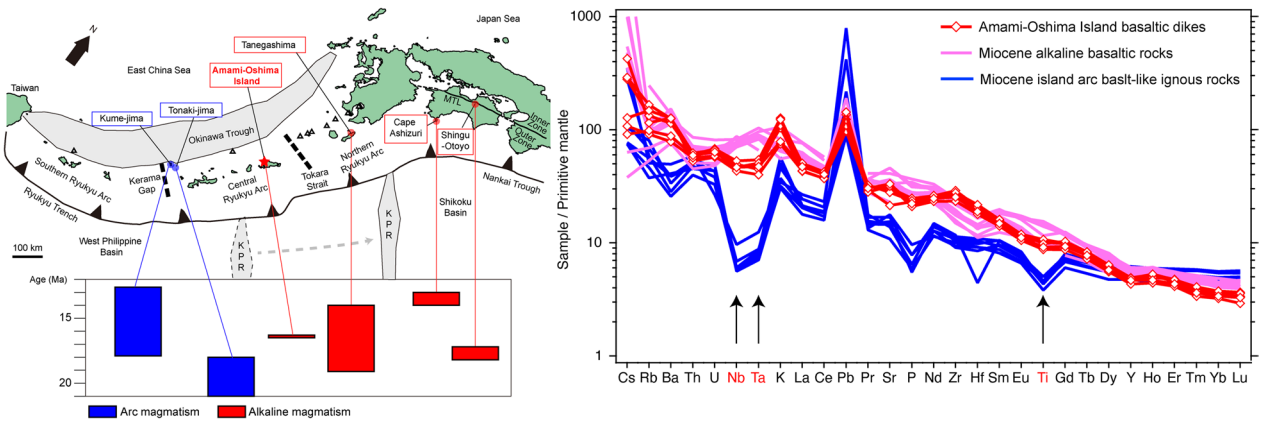

Introduction

During the middle Miocene, intensive magmatism occurred in Southwest Japan, resulting in the formation of high-magnesian andesites (HMA), felsic plutonic rocks, forearc mid-ocean ridge basalt (MORB)-like basalts, and forearc alkaline basalts (Kimura et al. 2005). This magmatism is thought to have occurred in association with the subduction of the young and hot Shikoku Basin (Kimura et al. 2005; Tatsumi 2006). Southwest Japan consists of Inner and Outer Zones, which are bounded by the Median Tectonic Line (Fig. 1a). In the southernmost part of the Inner Zone of Southwest Japan (Setouchi Province), the HMA was presumably formed by the interaction of slab melt with mantle peridotite (Tatsumi 2006). In the Outer Zone of Southwest Japan, HMA magma with crustal contamination and/or melts of subducted sediments resulted in felsic magmatism, while subduction generated MORB-like and forearc alkaline basaltic rocks (Kimura et al. 2005).

Lamprophyre dike, which has an alkaline basaltic composition, was found in Tanegashima (Taneda and Kinoshita 1972; Ogasawara 1997; Kiminami et al. 2017). The lamprophyre dike yields K–Ar ages of 16 ± 2 Ma (Taneda and Kinoshita 1972) and 18.2 ± 0.9 Ma (Ogasawara 1997), suggesting that forearc alkaline magmatism extended to the northern Ryukyu Arc (Kimura et al. 2005). On the other hand, Shinjo et al. (1999) proposed that arc volcanism occurred in the central Ryukyu Arc during 21–13 Ma. Therefore, the distribution of middle Miocene forearc alkaline magmatism is poorly constrained in the Ryukyu Arc.

In this paper, we present geological information, whole-rock composition, $^{40}Ar/^{39}Ar$ dating, and paleomagnetic directions of basaltic dikes on Amami-Oshima Island, central Ryukyu Arc. Based on these results, we discuss the timing of the basaltic dike intrusion and the magma origin of basaltic dikes. Our results provide an important constraint on the distribution of forearc alkaline magmatism in Southwest Japan and the Ryukyu Arc during the middle Miocene.

Geological background

Amami-Oshima Island is located in the central Ryukyu Arc between the Tokara Strait and the Kerama Gap, in which the geological belts are considered to be the southern extension of the Outer Zone of Southwest Japan (Wallis et al. 2020; Fig. 1a). The island consists of the Chichibu accretionary complex, Late Cretaceous Shimanto accretionary complex, Early Cretaceous lamprophyre, Eocene and Miocene granitic rocks, Eocene Wano Formation, and Quaternary sediments (Takeuchi 1993; Fig. 1b). The Chichibu accretionary complex in Amami-Oshima Island consists of a mélange characterized by blocks of chert, basalt, limestone, siliceous mudstone, and sandstone in the mudstone matrix (Takeuchi 1993). Although the accretionary age of the Chichibu accretionary complex remains unknown, correlation of geologic belts between Amami-Oshima Island and the Outer Zone of Southwest Japan and lithological assemblage of the mélange are comparable to the Late Jurassic to Early Cretaceous Chichibu accretionary complex in the Southwest Japan, which has been thought to represent the accretion of a seamount chain (Matsuoka 1992).

The basaltic rocks in the Chichibu accretionary complex of Amami-Oshima Island are exposed as blocks in the mudstone matrix. These blocks are composed of massive basalt, pillow basalt and breccia, hyaloclastite, and

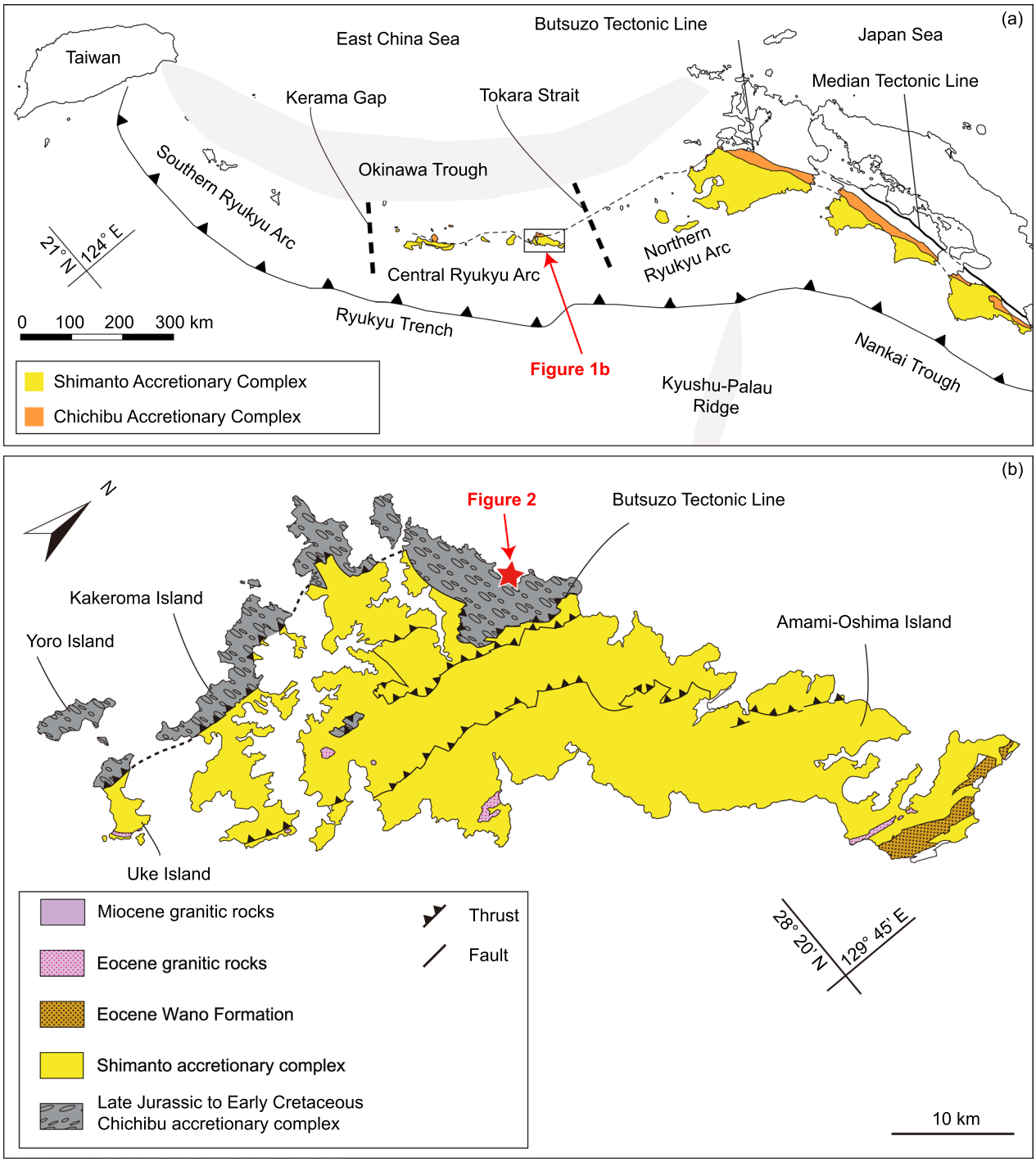

Fig. 1 Index map around the Ryukyu Arc. **a** The distribution of the Shimanto and Chichibu accretionary complexes in Southwest Japan and the Ryukyu Arc. Modified from Wallis et al. (2020). **b** Geological map of Amami-Oshima Island. Modified from Takeuchi (1993). The location of the figure is shown in **a**. The red star indicates the location of basaltic dikes at Naon

dolerite. Basalt blocks are also accompanied with chert and limestone. In addition, basaltic dikes, basaltic sills, and lamprophyre dikes intrude the Chichibu accretionary complex of Amami-Oshima Island (Kanisawa et al. 1983; Osozawa et al. 1983; Takeuchi 1993). Cretaceous lamprophyres, which have alkaline basaltic compositions, intrude into the pelagic sediments of the Chichibu accretionary complex of Amami-Oshima Island (Kanisawa

et al. 1983; Osozawa et al. 1983). The basaltic dikes investigated are located at Naon (Fig. 1b) in the Chichibu accretionary complex. These dikes were reported by Takeuchi (1993), but their chemical compositions and ages remain unknown.

Occurrence of basaltic dikes and massive basalt

At Naon on Amami-Oshima Island, two basaltic dikes of 35–80 cm in thickness sharply intrude massive basalt, reddish chert, varicolored shale, and grey chert (Fig. 2a, b). The dikes strike east–northeast and dip steeply north, whereas bedding in grey chert dips moderately east (Fig. 2a). The boundaries between the dike and grey chert are rounded and embayed, possibly representing the melting of the grey chert wall rock (Fig. 3a, b). The injection structures are observed in the chert. Chilled margins 1–2 mm thick with light grey or pale green color are recognized along the dike margins (Fig. 2c, d).

Under the microscope, the basaltic dikes are mainly composed of plagioclase, olivine, Fe–Ti oxide minerals, and interstitial glass with minor pyrite, apatite, and calcite (Fig. 3c). Olivine crystals (0.5–1 mm in size) and interstitial glass are commonly altered to chlorite, but plagioclase crystals (0.1–0.2 mm in size) are relatively

Fig. 2 Occurrence of basaltic dikes at Naon in Amami-Oshima Island. **a** Two basaltic dikes intrude massive basalt and grey chert in the mélange. **b** Basaltic dike cuts massive basalt, reddish chert, varicolored shale, and grey chert. **c** Contact between dike and chert. **d** Chilled margin preserved along the boundary between dike and massive basalt. Locations of panels **b**–**d** are shown in **a**

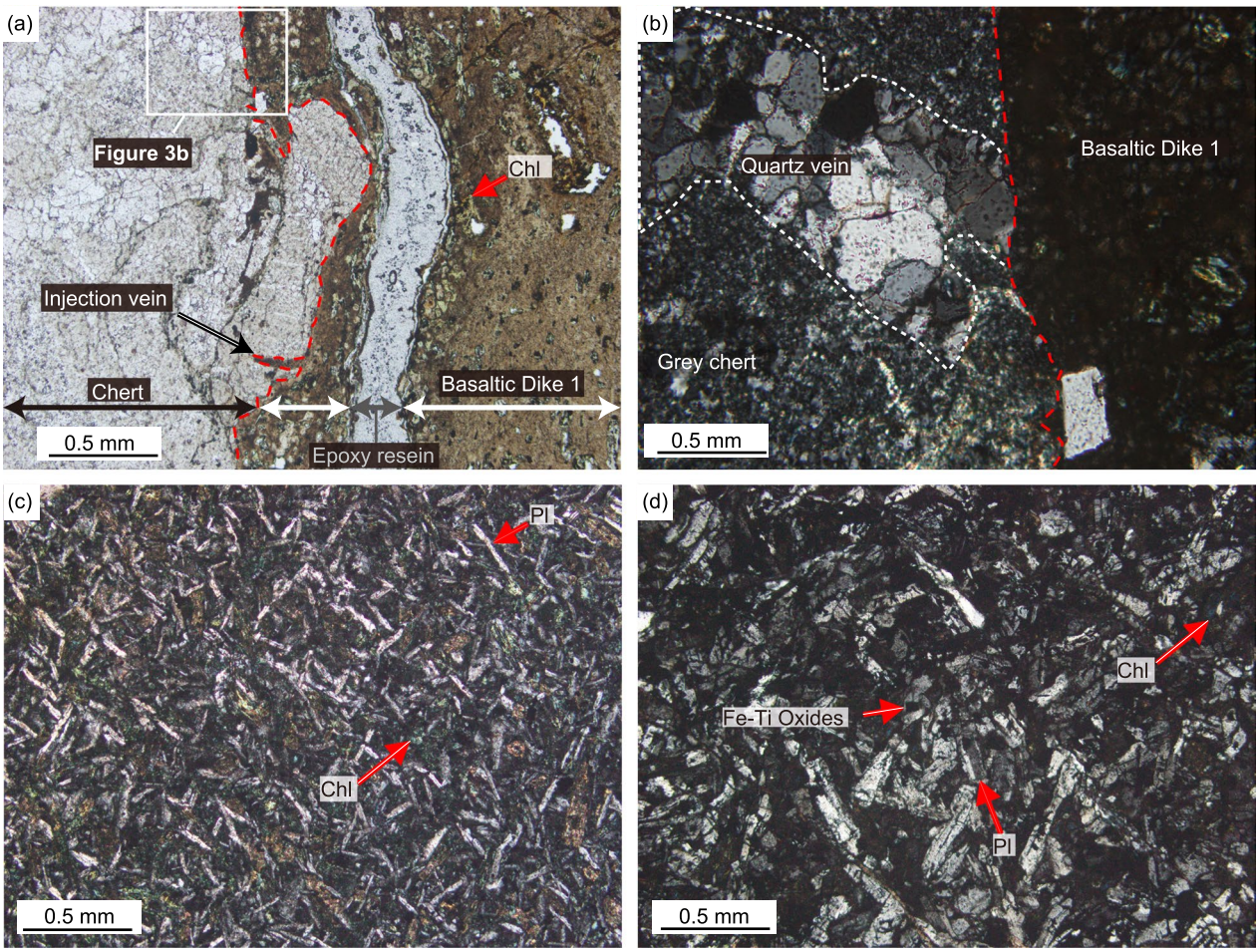

Fig. 3 Photomicrographs of the basaltic dikes and massive basalt. **a** Plane-polarized light and **b**, **c**, **d** cross-polarized light. **a** Outer margin of the basaltic dike is locally altered to chlorite (Chl). **b** The chert including quartz vein was cut by the basaltic dike. Location of the figure is shown in **a**. **c** Basaltic Dike 1 (NCD1-2) and **d** massive basalt (NC8). Pl: plagioclase, Fe–Ti oxides: Fe–Ti oxide minerals

fresh. Pyrite crystals (0.1–1 mm in size) are subhedral to anhedral, while apatite crystals (10–30 μm in size) are euhedral to subhedral. The outer margin of the dike preserved glass, but was locally altered to chlorite. The quartz veins in the grey chert were truncated by the dike (Fig. 3b), suggesting that the grey chert was lithified during dike intrusion. The massive basalt is mainly composed of 0.3–0.8 mm plagioclase crystals with Fe–Ti oxide minerals (0.05–0.2 mm in size), chlorite, and calcite (Fig. 3d). Interstitial glass is altered to chlorite and calcite veins are present. Olivine, pyrite, and apatite crystals are not recognized under the microscope.

Samples and methods

Samples

Samples for $^{40}Ar/^{39}Ar$ dating, geochemical, and paleomagnetic analyses were taken from two basaltic dikes and massive basalt at Naon on Amami-Oshima Island (Lat. = 28.332499°N, Long. = 129.30698910°E; Additional file 1: Figure S1). For the paleomagnetic study, 11 and 9 oriented hand samples were collected from Dike 1 and Dike 2, respectively (Additional file 1: Figure S1b). Each hand sample was marked by three points representing a reference plane with strike (relative to magnetic north and a line connecting the two marked points sharing the strike direction) and dip (represented by a line connecting the midpoint of the two marked points and the third marked point). In the laboratory, each hand sample was fixed with plaster to make the reference plane horizontal to take several cylindrical cores from each hand sample vertically with a boring machine. Each drilled core was cut perpendicular to the axis of the cylinder to prepare several cylindrical specimens (25 mm in diameter and 22 mm in length).

Methods

The analytical details are presented in Additional Text S1 and outlined here. The $^{40}Ar/^{39}Ar$ dating was conducted on acid-leached samples from two basaltic dikes (Additional file 2: Table S1). Neutron irradiation and Ar isotope measurements were conducted at the Kyoto University Reactor (KUR) and Geological Survey of Japan, National Institute of Advanced Industrial Sciences and Technology (AIST). Major and selected trace elements for ten less-altered samples from two basaltic dikes and massive basalt were measured using a Rigaku ZSX Primus II X-ray fluorescence (XRF) spectrometer at the National Museum of Nature and Science (NMNS). After XRF analysis, the concentration of a larger range of trace elements was measured using a quadrupole Agilent 7700 × inductively coupled plasma-source mass spectrometry (ICP-MS) instrument at the NMNS. Analytical precision data for XRF and ICP-MS, estimated from repeated analyses of a well-established reference standard (JB-1a), are given in Tables S2 and S3. The standard deviations of the calibration lines for the XRF are reported in Additional file 2: Table S2.

Paleomagnetic measurements were conducted at the GSJ-Lab. at AIST, using a superconducting rock magnetometer (2G Enterprises model 760) and a thermal demagnetizer (Natsuhara Giken TDS-1). The cylindrical specimens were subjected to the stepwise thermal demagnetization experiments (ThD) in air from 25 ℃ up to 600 ℃ over 24–30 steps. The results of the experiments were processed using Paleomagnetism.org 2.0 (Koymans et al. 2016, 2020). The characteristic remanent magnetization (ChRM) of the specimens was determined using principal component analysis (PCA: Kirschvink 1980), and paleomagnetic directions with maximum angular deviations (MAD) < 10° were adopted. The mean ChRM direction of each hand sample was then determined by the combined analyses of remagnetization circles (McFadden and McElhinny 1988; Additional file 1: Text S1.4). To identify the nature of the main magnetic carriers contributing to the primary remanent magnetizations, rock magnetic measurements were performed at the AIST Nano-Processing Facility (AIST-NPF) and GSJ-Lab. at AIST (see details in Additional file 1: Text S1.5).

Results

$^{40}Ar/^{39}Ar$ age of basaltic dikes

To evaluate the effects of alteration present in the low-temperature steps, the samples were subjected to 26 step-heating intervals by laser heating. Plateaus defined by 14 and 20 steps yield ages of 16.37 ± 0.14 Ma and 16.51 ± 0.10 Ma for NCD1-2 (Dike1) and NCD2-2 (Dike2) samples, respectively (Additional file 1: Figure S2; Additional file 2: Table S1). The plateaus comprised 53.8 and 84.5% of the released gas from NCD1-2 and NCD2-2, respectively. In addition, both samples returned well-defined isochrons with $^{36}Ar/^{40}Ar$ intercepts identical to the atmospheric ratio within a 2σ error, and the derived isochron ages were 16.57 ± 0.28 Ma and 16.56 ± 0.24 Ma for NCD1-2 and NCD2-2 samples, respectively. For each sample, the weighted average age of the plateau-forming steps and the isochron age were identical within 2σ error ranges. Therefore, the ages of 16.37 ± 0.14 Ma and 16.51 ± 0.10 Ma were regarded as reliable intrusion ages for NCD1-2 and NCD2-2, respectively. The obtained ages of basaltic dikes both indicate the middle Miocene and are indistinguishable within a 2σ error.

Geochemical features of basaltic rocks

The basaltic dikes have basaltic trachyandesite and trachyandesitic compositions, whereas the massive basalts have a wide compositional range from basalt to basaltic trachyandesitic to trachyandesitic compositions (Fig. 4a, Additional file 2: Tables S2, and S3). In the discrimination diagram using Th and Nb, both basaltic dikes and massive basalts plot near the ocean island basalt (OIB) within the field of alkaline basalt (Fig. 4b).

In the primitive mantle (PM; Sun and McDonough 1989) normalized trace element pattern (Fig. 5a), both the basaltic dikes and the massive basalt are characterized by enrichment in large-ion lithophile (LIL) elements and light rare earth elements (REE), similar to OIB. The trace element abundances of Dike 1 and Dike 2 were almost the same, except for fluid-mobile elements such as Cs, Rb, Ba, K, and Pb, possibly due to the difference in the degree of alteration rather than the original magma compositions. The massive basalts show enrichment of Nb and Ta with depletion of Zr and Hf compared to the basaltic dikes (Fig. 5a). The PM-normalized trace element patterns of basaltic dikes resemble those of the Miocene alkaline basaltic rocks in Tanegashima and the Outer Zone of Southwest Japan, but differ from those of the island arc basalt-like rocks in the central Ryukyu Arc (Fig. 5b, c).

Paleomagnetism

The results of stepwise ThD show three to four linear components in the Zijderveld (vector endpoint) diagrams (Zijderveld 1967) for basaltic Dike 1 and Dike 2 (Additional file 1: Figure S3). Components were classified into four groups based on the temperature ranges, i.e., 25–100 °C (component A), 100–300 °C (component B), 300–425 °C (component C), and 450–575 °C (component D). As the directions of components A, B, and C were scattered, they were considered secondary origins and possibly related to alteration. The directions of component D exhibited a stable linear trend towards the origin

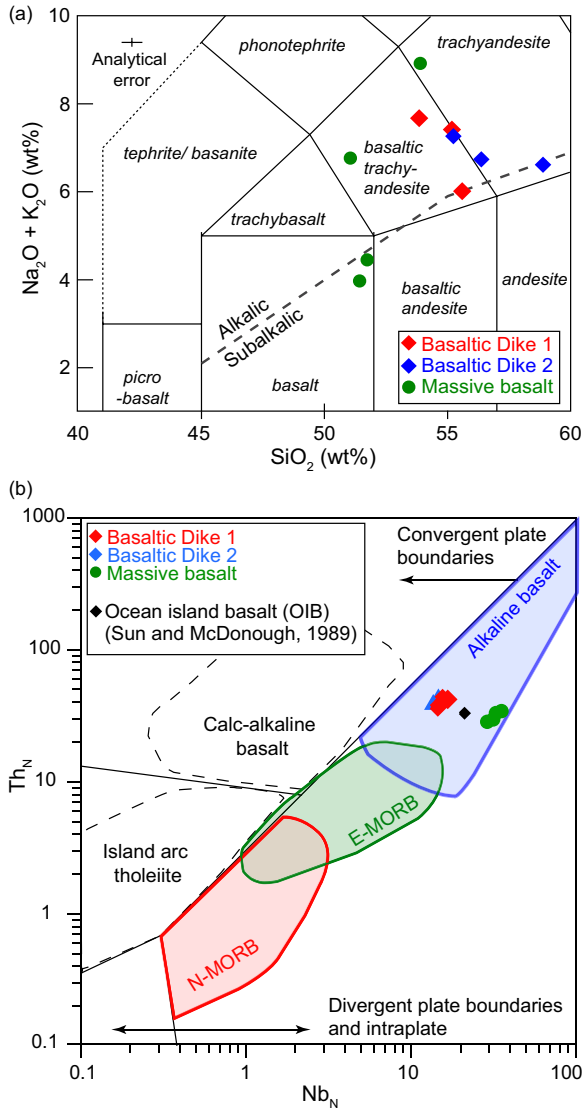

Fig. 4 Geochemical discrimination diagram of basaltic rocks in Amami-Ohshima Island. **a** Total alkali vs. SiO_2 plot (after Le Maitre 2002). The dashed line separates alkalic and subalkalic rocks from Miyashiro (1978). Error bars indicate standard deviations (two sigma) for calibration lines of the XRF analyses (Additional file 2: Table S2). **b** Geochemical discrimination diagram using Th and Nb. Modified from Saccani (2015). Subscript 'N' refers to values normalized to normal mid-ocean ridge basalt (N-MORB). E-MORB: Enriched MORB. The two standard deviations of repeated sample analyses are less than the size of the symbols (Additional file 2: Table S3)

(see the insets of Additional file 1: Figure S3c). Component D shared a common direction of negative inclination at approximately 25% and 75% of the specimens in Dike 1 and Dike 2, respectively (Additional file 2: Table S4). After PCA and the combined analyses of remagnetization circles (see Additional file 1: Text S1.4 and Figure S4), reliable paleomagnetic directions were obtained from three and eight hand samples of Dike 1 and Dike 2, respectively (Additional file 2: Table S5). The parameters for fitting the stepwise ThD results for component D are summarized in Additional file 2: Table S4. The average paleomagnetic directions of the hand samples yielded mean ChRM directions with negative inclinations (Additional file 1: Figure S5a, b). The mean direction of Dike 2 (declination; $D = 124.0°$, inclination; $I = -24.9°$, $\alpha_{95} = 8.1°$) was within the 95% confidence limit for that of Dike 1 ($D = 138.1°$, $I = -13.3°$, $\alpha_{95} = 18.3°$) (Additional file 1: Figure S5c). The virtual geomagnetic poles (VGPs) for Dike 1 and Dike 2 are in the southern hemisphere, whose latitudes are slightly $< 45°$ (Fig. 6a).

Discussion

Middle Miocene forearc alkaline magmatism in Amami-Oshima Island

The $^{40}Ar/^{39}Ar$ ages of basaltic dikes were 16.37 ± 0.14 Ma and 16.51 ± 0.10 Ma (Additional file 1: Figure S2 and Additional file 2: Table S1). This indicates that basaltic dike intrusion occurred in the accretionary complex during the middle Miocene, much younger than inferred accretionary age of Late Jurassic to Early Cretaceous. In contrast, the massive basalt intruded by the basaltic dikes was overlain by pelagic sedimentary rock. The massive basalt shows OIB-like trace element patterns with distinctive enrichment of Nb and Ta and depletion of Zr and Hf (Fig. 5a). Similar OIB-like basaltic rocks were also reported from the Chichibu accretionary complex of southwest Japan, which are interpreted to originate from intraplate volcanism associated with plume activity (e.g., Tatsumi et al. 2000; Onoue et al. 2004; Safonova et al. 2015). Similarly, the massive basalt at Naon likely represents intraplate volcanism before subduction.

Paleomagnetic analyses show that basaltic dikes have three to four linear components. The stable ChRM, obtained at 450–575 °C, is considered the primary magnetization at the time of the basaltic dike intrusions and

(See figure on next page.)

Fig. 5 Primitive mantle normalized trace element patterns of basaltic rocks in Amami-Oshima Island. Trace element patterns of basaltic rocks in Amami-Oshima Island in comparison with **a** OIB, N-MORB, and E-MORB; **b** Miocene alkaline basaltic rocks; and **c** island arc basalt-like rocks. Data for Miocene rocks were compiled from the following sources: Kiminami et al. (2017) for Tanegashima, Otoyo, and Shingu; Shinjoe et al. (2003) for Cape Ashizuri; and Shinjo et al. (1999) for Kume-jima and Tonaki-jima. Data for N-MORB and E-MORB are obtained from Gale et al. (2013). The primitive mantle values were obtained from Sun and McDonough (1989). Note that HFSE such as Nb, Ta, and Ti (highlighted in red) are depleted in volcanic rocks in Kume-jima and Tonaki-jima, but not depleted in basaltic dikes on Amami-Oshima Island

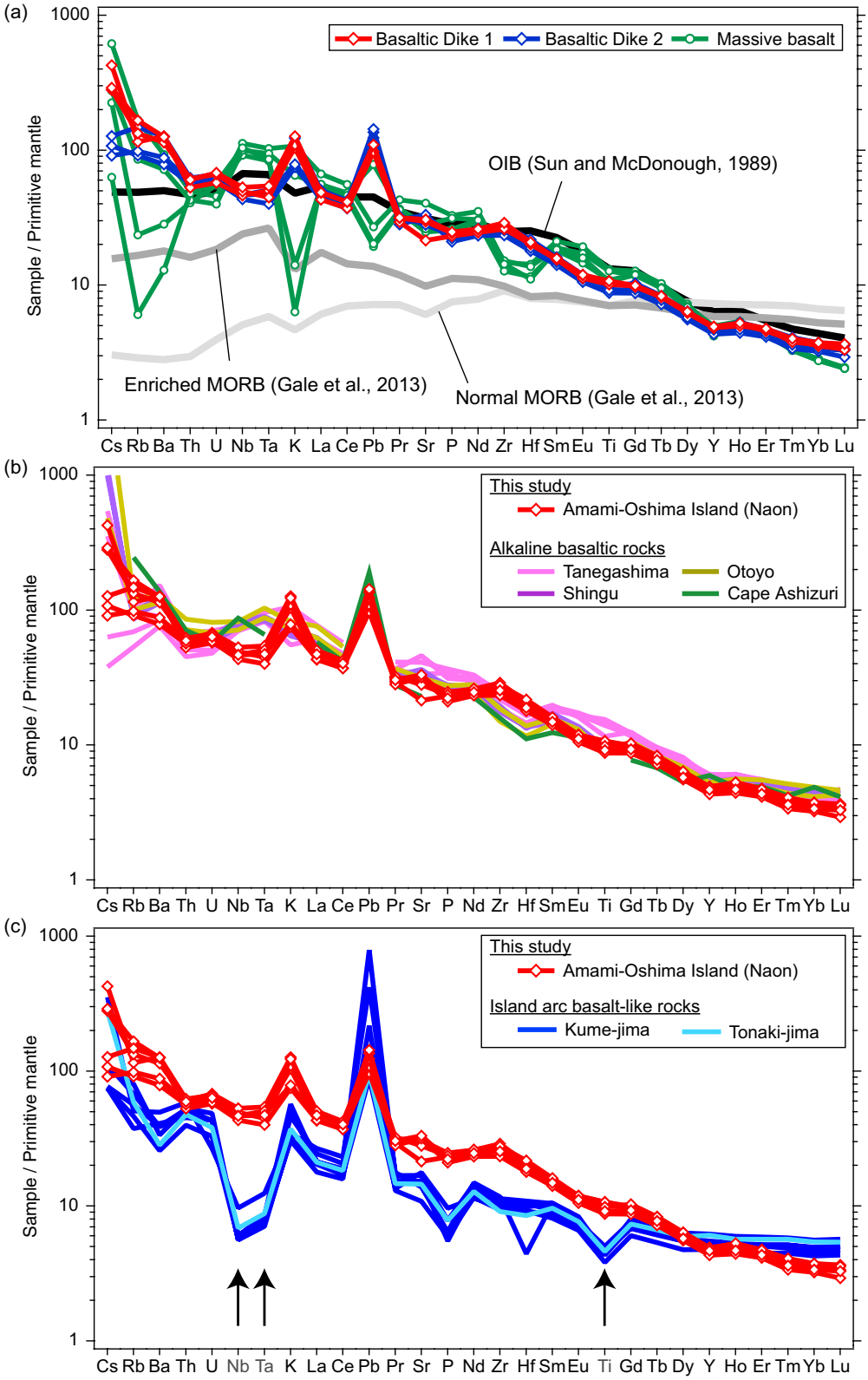

Fig. 5 (See legend on previous page.)

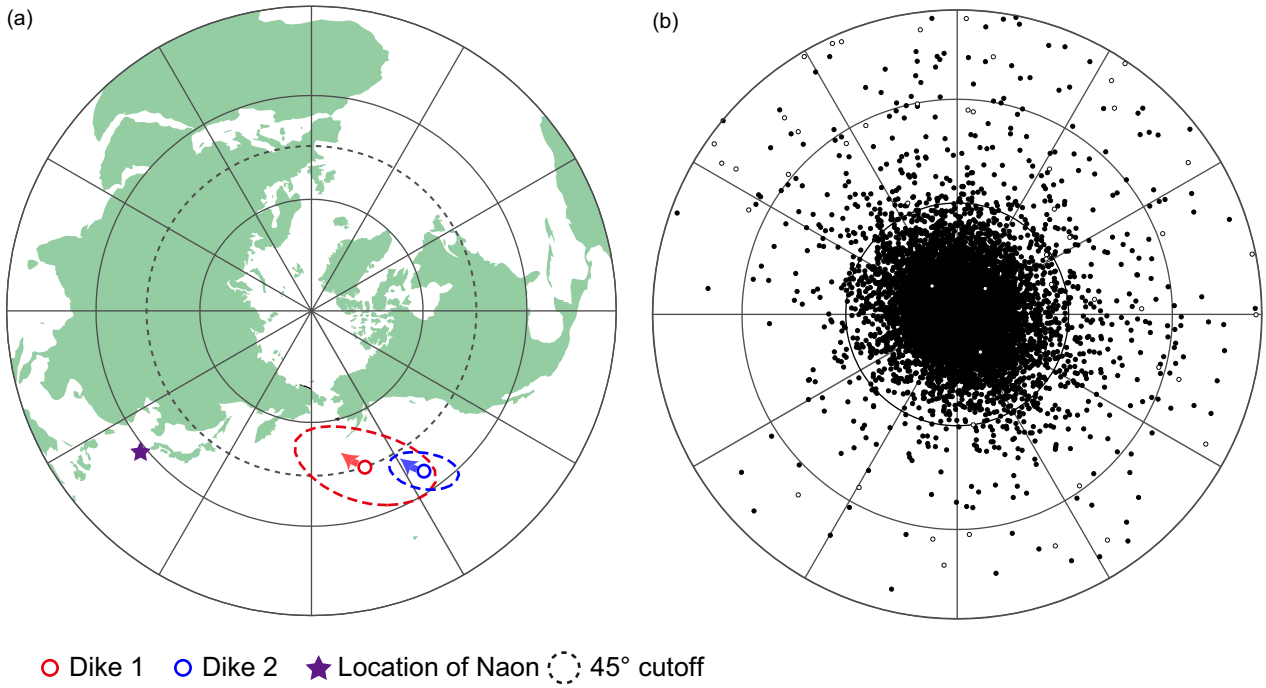

Fig. 6 **a** VGP of Dike1 and Dike2. **b** VGP distributions for paleosecular variation at the site. **a** An equal area projection of mean paleomagnetic directions. Note that VGPs projected onto the southern hemisphere are shown as open circles. A purple star indicates the location of Naon (129.31 °E, 28.33 °N). Light red and light blue arrows indicate VGP latitudes for Dike1 and Dike2 corrected for ~ 5 ° CW rotation, respectively. **b** VGPs for 10,000 paleomagnetic directions for the studied site by random sampling based on the secular variation model of TK03.GAD (Tauxe and Kent 2004) using python code tk03.py of pmagpy (https://earthref.org/MagIC/books/Tauxe/Essentials/). TK03.GAD model is based on PSVRL (paleosecular variation from lavas) database (see McElhinny and McFadden (1997)). Solid (open) circles are VGPs plotted onto the northern (southern) hemisphere. Using the simulated paleosecular variations, we estimated the probability of having the paleomagnetic directions for Dike1 and Dike2. The probability of having the paleomagnetic directions for dike1 within 17.6 ° angular distance (calculated from the paleomagnetic directions for the two dikes; see Fig. 5a) from dike2 by chance is 0.3%

is carried by magnetite with a small fraction of Ti substitution and/or non-stoichiometry (see Additional file 1: Text S2). The primary magnetization yielded mean paleomagnetic directions with negative inclinations (Additional file 1: Figure S5c). The latitudes of the associated VGPs were almost equal to or slightly lower than 45 ° (45°S for Dike 1 and 36°S for Dike 2; Fig. 6a).

The probability that the basaltic intrusion event occurred during the polarity transitions and excursions was < 2% and 3%, respectively (see Additional file 1: Text S3). We further investigated the possibility that the basaltic dikes experienced tectonic rotations after the intrusion over the past 2 Ma. Nishimura et al. (2004) suggested a counterclockwise (CCW) rotation of 3.95×10^{-2} rad/Myr for the central Ryukyu Arc, including Amami-Oshima Island, using GPS data from 37 stations during 1996–2001. Assuming a constant rotation associated with the spreading of the Okinawa Trough in the past 2 Ma, this corresponds to a CCW rotation of ~ 5° for the total period. A correction of ~ 5° clockwise (CW) rotation gives VGP latitudes of 49° S for Dike 1 and 40° S for Dike 2 (light blue and light red arrows in Fig. 6a), whose confidence limits overlap with the 45° cutoff angle. Thus, we suggest that the paleomagnetic directions for the two dikes were acquired either as part of the secular variation or a geomagnetic excursion during the reversed polarity chron/subchron. We consider that the probabilities that the paleomagnetic directions were recordings of a paleomagnetic field during a polarity transition or a reversal excursion during a normal polarity chron/subchron are low.

Compared with corresponding age interval of Geologic Time Scale 2020 for the Neogene Period (Raffi et al. 2020), which is taken from astronomically tuned age for U1336 (Kochhann et al. 2016), the $^{40}Ar/^{39}Ar$ ages of the basaltic dikes overlap with the chrons of C5Cn and C5Cr (17.466–15.994 Ma) within a 2σ error range. Please note that the ages in the summary table of Ogg (2020) for Geomagnetic Polarity Timescale 2020 has errors for Chrons C5B, C5C, and C5D. Assuming that the scenario in the previous paragraph was valid, the ChRMs for the two dikes were acquired during a reversed chron/subchron.

Within a 2σ error range, the $^{40}Ar/^{39}Ar$ age of one dike (16.37 ± 0.14 Ma) overlaps with the subchrons of C5Cn.1r (16.351–16.261 Ma) and C5Cn.2r (16.532–16.434 Ma), whereas that of the other dike (16.51 ± 0.10 Ma) overlaps with C5Cn.2r and chron C5Cr (17.154–16.637 Ma) (Fig. 7). The two basaltic dikes have almost the same trace element concentrations (Fig. 5), and the $^{40}Ar/^{39}Ar$ ages were identical within a 2σ error range (Additional file 1: Figure S2). In addition, examination of the paleosecular variations suggests that paleomagnetic directions for dikes are unlikely to be obtained independently (probability is 0.3% for uncorrected paleomagnetic directions; see the caption of Fig. 6). These features suggest that the intrusions of the two basaltic dikes occurred at almost the same time. Thus, the intrusion of basaltic dikes on Amami-Oshima Island is likely to have occurred during C5Cn.2r (16.532–16.434 Ma).

Implications for along-arc variation of magmatism in central Ryukyu Arc

The geochemical, geochronological, and paleomagnetic results of the basaltic dikes suggest the presence of middle Miocene forearc alkaline magmatism in Amami-Oshima Island, central Ryukyu Arc. Between 18–13 Ma, intrusion events of alkaline basaltic rocks have been reported from Tanegashima in the northern Ryukyu Arc (Taneda and Kinoshita 1972; Ogasawara 1997; Kiminami et al. 2017) and the Outer Zone of Southwest Japan (Uto et al. 1987; Shinjoe et al. 2003, 2010; Kiminami et al. 2017, Matsumoto et al. 2020). These alkaline basaltic rocks are considered to have formed in the forearc region as a part of Miocene igneous activity associated with the subduction of the young and warm Shikoku Basin (e.g., Kimura et al. 2005). The ages and trace element patterns of basaltic dikes on Amami-Oshima Island are comparable to those of the alkaline basaltic rocks in Tanegashima and the Outer Zone of Southwest Japan (Figs. 5b and 8), suggesting that the forearc alkaline magmatism during the Miocene may have extended to Amami-Oshima Island in the central Ryukyu Arc.

On the other hand, arc magmatism of 21–13 Ma was recorded in basaltic to dacitic rocks from Kume-jima and Tonaki-jima in the southern part of the central Ryukyu Arc (Shinjo et al. 1999). These rocks were characterized by the depletion of high-field-strength elements (HFSE), such as Nb, Ta, and Ti in the PM-normalized trace element patterns (Fig. 5c). Low concentrations of HFSE are characteristic of typical arc magmas derived from wedge mantle that are depleted in HFSE (e.g., Zheng 2019). To explain arc magmatism, Shinjo et al. (1999) proposed the

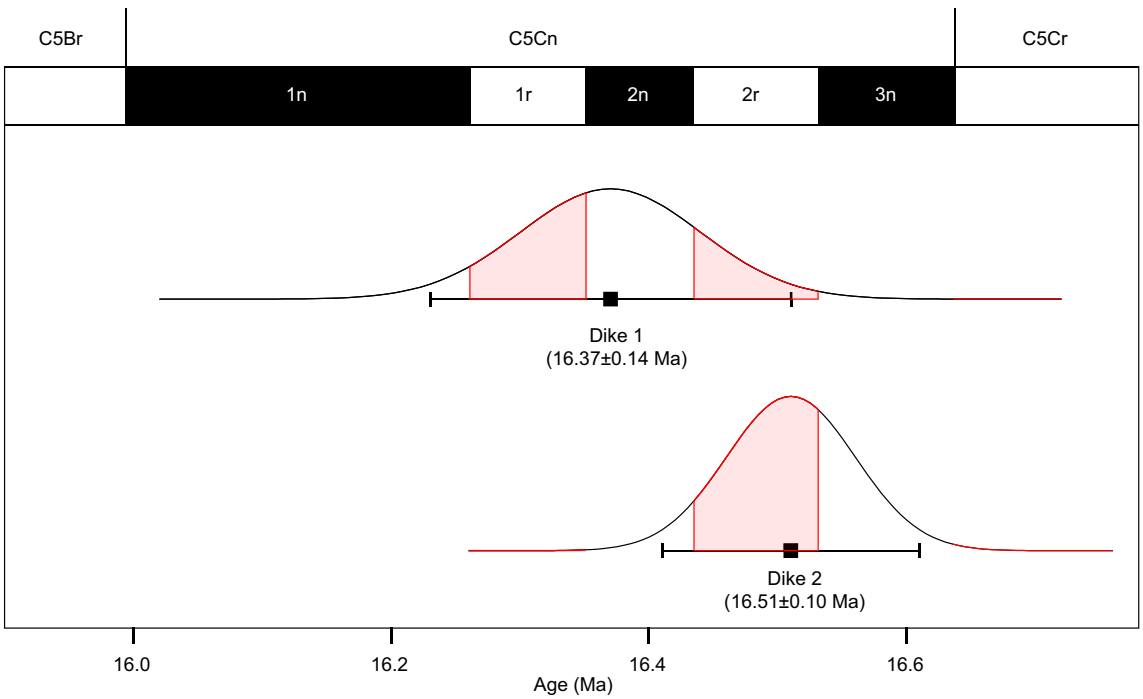

Fig. 7 $^{40}Ar/^{39}Ar$ ages of basaltic dikes correlated with the geomagnetic polarity timescale. The geomagnetic polarity timescale was obtained from Raffi et al. (2020). Curves indicate the probability density distribution calculated using the averages and standard deviations of the $^{40}Ar/^{39}Ar$ age of the basaltic dikes. Reddish shaded areas represent probabilities corresponding to the reversed polarity subchrons C5Cn.1r and C5Cn.2r, and the chron of C5Cr

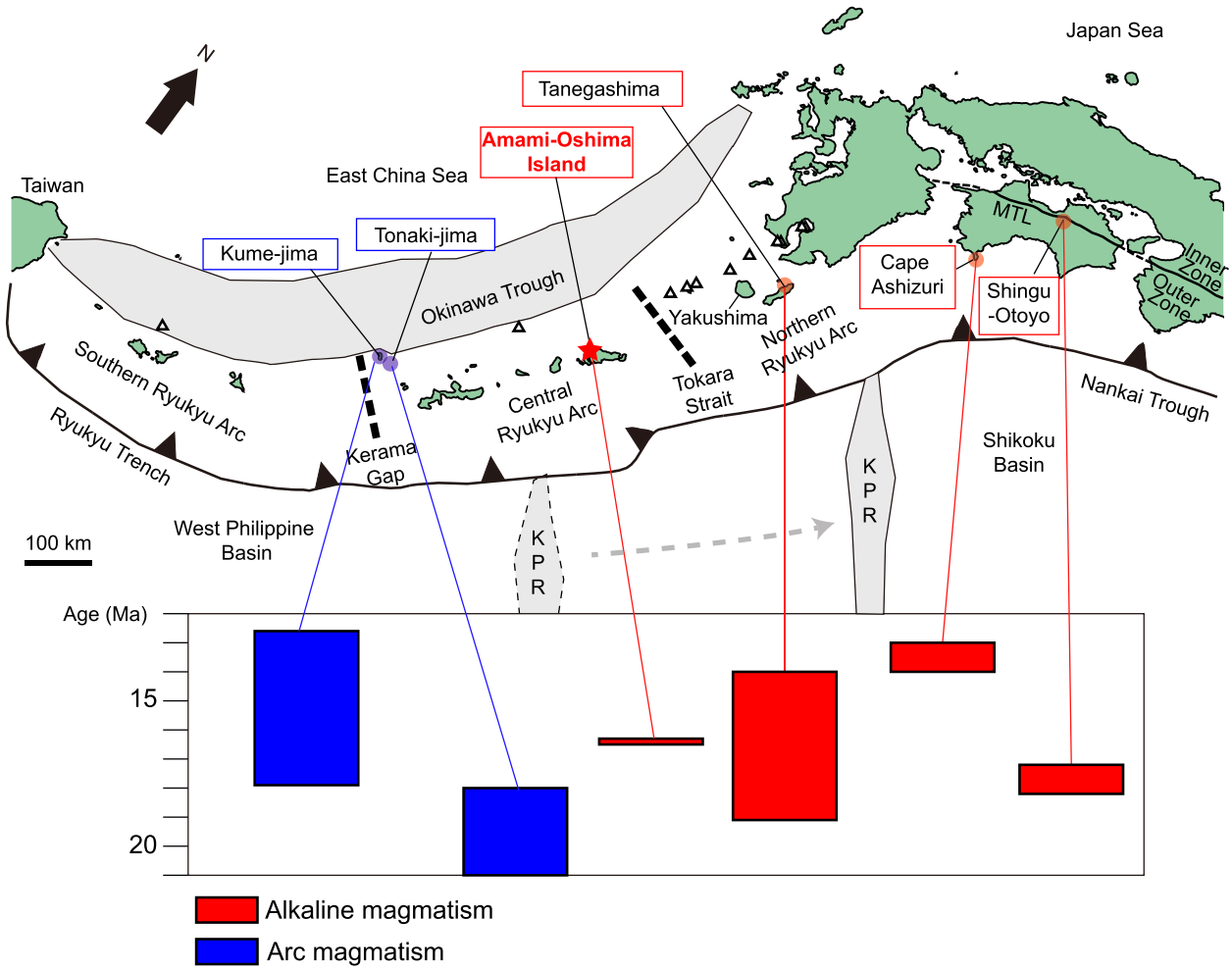

Fig. 8 Age and distribution of forearc alkaline (red) and arc (blue) magmatism during middle Miocene. MTL: Median Tectonic Line, KPR: Kyushu-Palau Ridge. The white open triangle indicates Quaternary volcanoes on the volcanic front of Shinjo and Kato (2000). The red and blue symbols represent the alkaline and arc magnetism, respectively. The red star represents the study site. Age ranges for Miocene magmatism were compiled from the following sources: Uto et al. (1987) for the Shingu-Otoyo area; Shinjoe et al. (2010), and Matsumoto et al. (2020) for Cape Ashizuri; Ogasawara (1997) and Taneda & Kinoshita (1972) for Tanegashima; Daishi et al. (1987), Miki (1995), and Nakagawa and Murakami (1975) for Kume-jima; Kato (1985) for Tonaki-jima. The area enclosed by the broken line represents the paleo-location of the Kyushu-Palau Ridge in the middle Miocene, inferred from along the arc variation of magmatism in the central Ryukyu Arc

subduction of the Philippine Sea plate beneath the central Ryukyu Arc during the middle Miocene. However, the basaltic dikes on Amami-Oshima Island do not have such a depletion, implying that they do not comprise typical arc magma. Therefore, two different styles of magmatism (forearc alkaline magmatism and arc magmatism in the north and south, respectively) were present in the central Ryukyu Arc during the middle Miocene (Fig. 8).

The difference in magmatism along the central Ryukyu Arc could represent a difference in the subducting plate: the Shikoku Basin in the north and the West Philippine Basin in the south. The Shikoku Basin was formed along a ridge between the Izu-Bonin Arc and Kyushu-Palau Ridge between 27 and 15 Ma (Okino et al. 1999; Okino 2015), whereas the West Philippine Basin was formed in the western part of the Philippine Sea Plate between 50 and 36 Ma (Sasaki et al. 2014). The opening of the Japan Sea between 18 and 16 Ma with clockwise rotation of Southwest Japan (Hoshi 2018) is considered to have initiated the subduction of the Shikoku Basin beneath the Japanese Islands (Tatsumi and Hanyu 2003).

While the young and warm Shikoku Basin began to subduct beneath the Eurasian Plate, the relatively old and cold West Philippine Basin subduction had already progressed in the southern part of the central Ryukyu Arc. Under such conditions, forearc alkaline magmatism may have occurred in association with the subduction of the young Shikoku Basin, whereas arc magmatism may have

been caused by dehydration from the subducted old West Philippine Basin (Shinjo et al. 1999). Thus, the northern end of the Kyushu-Palau Ridge may have been located between Amami-Oshima Island and Kume-jima/Tonaki-jima around 16.5–16.4 Ma before migrating eastward to present location (Fig. 8). Tatsumi et al. (2020) proposed that the northern end of the Kyushu-Palau Ridge was located south of Yakushima Island at ca. 14 Ma based on the age of granitic plutonism in Yakushima Island. However, the age of alkaline basaltic dikes at Naon implies that the Kyushu-Palau Ridge may be located to the west of Amami-Oshima Island during the middle Miocene.

Conclusions

Geochemical, geochronological, and paleomagnetic investigations were conducted on the two basaltic dikes in the Chichibu accretionary complex of Amami-Oshima Island, central Ryukyu Arc. The basaltic dikes have incompatible trace elements-enriched alkaline basaltic compositions and yielded the $^{40}Ar/^{39}Ar$ ages of 16.37 ± 0.14 Ma and 16.51 ± 0.10 Ma, indicative of an alkaline basaltic dike intrusion during the middle Miocene. Paleomagnetic analyses suggest that the primary paleomagnetic directions for the two dikes were acquired either as part of a secular variation or a geomagnetic excursion during the reversed polarity chron/subchron. $^{40}Ar/^{39}Ar$ age of one dike overlaps with the subchrons of C5Cn.1r (16.351–16.261 Ma) and C5Cn.2r (16.532–16.434 Ma), whereas that of the other dike overlaps with C5Cn.2r and chron C5Cr (17.466–17.154 Ma). The two basaltic dikes are indistinguishable by geochemical compositions, ages, and paleomagnetic directions within the error range, implying that they are likely to have intruded almost simultaneously during C5Cn.2r (16.532–16.434 Ma). The age and trace element patterns of the basaltic dikes are comparable to those of alkaline basaltic intrusive rocks distributed in the Outer Zone of Southwest Japan and the northern Ryukyu Arc. The discovery of alkaline basaltic dikes from Amami-Oshima Island suggests that the distribution of middle Miocene forearc alkaline magmatism may extend to the northern part of the central Ryukyu Arc. Hence, the northern end of the Kyushu-Palau Ridge could have been located south of Amami-Oshima Island around 16.5–16.4 Ma, then moved eastward to the current location.

Abbreviations

AIST	National Institute of Advanced Industrial Sciences and Technology
AGM	Alternating gradient magnetometer
Chl	Chlorite
ChRM	Characteristic remanent magnetization
CW	Clockwise
CCW	Counterclockwise
FC	Field cooling
Fe–Ti oxides	Fe–Ti oxide minerals
FORC	First-order remanent curve
HFSE	High-field strength element
HMA	High magnesian andesite
ICP-MS	Inductively coupled plasma-source mass spectrometry
IRM	Isothermal remanent magnetization
KUR	Kyoto University Reactor
LOI	Loss on ignition
MAD	Maximum angular dispersion
MD	Multi-domain
MORB	Mid-ocean ridge basalt
MPMS	Magnetic property measurement system
NMNS	National Museum of Nature and Science
NRM	Natural remanent magnetization
OIB	Ocean Island Basalt
PCA	Principal component analysis
Pl	Plagioclase
PM	Primitive mantle
PSD	Pseudo-single-domain
SD	Single-domain
ThD	Thermal demagnetization experiment
VGP	Virtual geomagnetic poles
VSM	Vibrating sample magnetometer
XRF	X-ray fluorescence
ZF	Zero-field
ZFC	Zero-field cooling

Supplementary Information

The online version contains supplementary material available at https://doi.org/10.1186/s40623-022-01760-w.

Additional file 1. Text S1–S3, Figure S1–S9, and additional references.

Additional file 2. Table S1–S5.

Acknowledgements

We appreciate Youko Kusaba for her assistance using a SELFLAG lab at NMNS. We would like to thank Ryo Okumura, Hisao Yoshinaga, and Yuto Iinuma for irradiation of dated samples at KUR, Institute for Integrated Radiation and Nuclear Science, Kyoto University. We thank Brad Dodrill for conducting isothermal remanent magnetization (IRM) measurements of 5 basaltic dike samples using a vibrating sample magnetometer (VSM) at Lake Shore Cryotronics, Inc. We also thank Ayako Katayama and Emiko Miyamura for assistance in using a superconducting rock magnetometer, a susceptibility meter, and a thermal demagnetizer at GSJ Lab., AIST. A part of this work was conducted at the AIST Nano-Processing Facility supported by "Nanotechnology Platform Program" of the Ministry of Education, Culture, Sports, Science and Technology (MEXT), Japan Grant Number JPMXP09F21009520. Most of the measurements and analyses on paleomagnetism and rock magnetism were made in GSJ Lab., AIST as a research assistant at AIST. We are grateful for the thoughtful and helpful comments by the two anonymous reviewers and for the EPS Editor, Katsuya Kaneko, and Editor-in-Chief, Takeshi Sagiya for the evaluation.

Author contributions

GM designed this study. GM wrote the paper with discussion and input from all authors. GM and HO prepared the figures. GM and KU carried out fieldwork. GM collected and prepared samples for geochemical, geochronological, paleomagnetic, and rock magnetic analyses. SS conducted neutron irradiation of samples for $^{40}Ar/^{39}Ar$ dating analysis. OI conducted $^{40}Ar/^{39}Ar$ dating analysis. GM and HO conducted paleomagnetic and rock magnetic measurements. GM and TS conducted major and trace element analyses. All authors read and approved the final version of the manuscript.

Funding

This project has received funding from Japan Society for the Promotion of Science KAKENHI grant 17K05686 to OI, 18H03746 to OI and TS, 18H05447 to TS, 20KK0082 and 21H04523 to HO, and JP16H06476, 20KK0078, 20K21050, and 21H05203 to KU.

Availability of data and materials
The data that support the findings in the present study are available from the corresponding author upon request.

Declarations

Ethics approval and consent to participate
Not applicable.

Consent for publication
Not applicable.

Competing interests
The authors declare that they have no competing interests.

Author details
[1]Graduate School of Science and Technology, University of Tsukuba, 1-1-1 Tennodai, Tsukuba, Ibaraki 305-8572, Japan. [2]Geological Survey of Japan, National Institute of Advanced Industrial Science and Technology, Central 7, 1-1-1 Higashi, Tsukuba, Ibaraki 305-8567, Japan. [3]Department of Geology and Paleontology, National Museum of Nature and Science, 4-1-1 Amakubo, Tsukuba, Ibaraki 305-0005, Japan. [4]Institute for Integrated Radiation and Nuclear Science, Kyoto University, 2 Asashironishi, Kumatori, Sennan, Osaka 590-0494, Japan. [5]Graduate School of Science and Technology, University of Tsukuba, 1-1-1 Tennodai, Tsukuba, Ibaraki 305-8572, Japan. [6]INPEX Corporation, Akasaka Biz Tower, 5-3-1 Akasaka, Minato-Ku, Tokyo 107-6332, Japan.

Received: 15 September 2022 Accepted: 25 December 2022
Published online: 19 January 2023

References

Daishi M, Hayashi M, Kato Y (1987) Radio-metric ages of some Cenozoic volcanic rocks from Ryukyu Islands. J Jpn Assoc Miner Petrol Econ Geol 82(10):370–381. https://doi.org/10.2465/ganko1941.82.370
Gale A, Dalton CA, Langmuir CH, Su Y, Schilling J (2013) The mean composition of ocean ridge basalts. Geochem Geophys Geosystems 14(3):489–518. https://doi.org/10.1029/2012GC004334
Hoshi H (2018) Miocene clockwise rotation of Southwest Japan. J Geol Soc Japan 124(9):675–691. https://doi.org/10.5575/geosoc.2017.0056
Kanisawa S, Osozawa S, Nakagawa H (1983) Petrology of Mesozoic lamprophyres in Amami-Oshima, Kagoshima Prefecture Japan. J Miner Petrol Econ Geol 78(10):394–404. https://doi.org/10.2465/ganko1941.78.394
Kiminami K, Imaoka T, Ogura K, Kawabata H, Ishizuka H, Mori Y (2017) Tectonic implications of early Miocene OIB magmatism in a near-trench setting: the outer zone of SW Japan and the northernmost Ryukyu Islands. J Asian Earth Sci 135:291–302. https://doi.org/10.1016/j.jseaes.2016.12.033
Kimura JI, Stern RJ, Yoshida T (2005) Reinitiation of subduction and magmatic responses in SW Japan during Neogene time. Geol Soc America Bull 117(7–8):969–986. https://doi.org/10.1130/B25565.1
Kirschvink JL (1980) The least-squares line and plane and the analysis of palaeomagnetic data. Geophys J Int 62(3):699–718. https://doi.org/10.1111/j.1365-246X.1980.tb02601.x
Kochhann KGD, Holbourn A, Kuhnt W, Channell JET, Lyle M, Shackford JK, Wilkens RH, Andersen N (2016) Eccentricity pacing of eastern equatorial pacific carbonate dissolution cycles during the Miocene climatic optimum. Paleoceanography 31(9):1176–1192. https://doi.org/10.1002/2016PA002988
Koymans MR, Langereis CG, Pastor-Galán D, van Hinsbergen DJJ (2016) Paleomagnetism.org: an online multi-platform open source environment for paleomagnetic data analysis. Comput Geosci 93:127–137. https://doi.org/10.1016/j.cageo.2016.05.007
Koymans MR, van Hinsbergen DJJ, Pastor-Galan D, Vaes B, Langereis CG (2020) Towards FAIR paleomagnetic data management through paleomagnetism.org 2.0. Geochem Geophys Geosystems 21(2):e2019GC008838. https://doi.org/10.1029/2019GC008838
Le Maitre RW (ed) (2002) Igneous rocks: a classification and glossary of terms: recommendation of the international union of geological sciences subcommission on the systematics of igneous rocks, 2nd edn. Cambridge Univ Press, Cambridge
Lowrie W (1990) Identification of ferromagnetic minerals in a rock by coercivity and unblocking temperature properties. Geophys Res Lett 17(2):159–162. https://doi.org/10.1029/GL017i002p00159
Matsumoto T, Aoki K, Windley BF, Aoki S (2020) The Ashizuri granite-alkaline gabbro complex in the forearc of a Paleogene accretionary complex, Shikoku, Japan: constraints on evolution by zircon U-Pb age and trace element composition. Geochem J 54(6):411–420. https://doi.org/10.2343/geochemj.2.0611
Matsuoka A (1992) Jurassic-early cretaceous tectonic evolution of the Southern Chichibu terrane, southwest Japan. Palaeogeogr Palaeoclimatol Palaeoecol 96(1):71–88. https://doi.org/10.1016/0031-0182(92)90060-I
McElhinny MW, McFadden PL (1997) Palaeosecular variation over the past 5 Myr based on a new generalized database. Geophys J Inter 131(2):240–252. https://doi.org/10.1111/j.1365-246X.1997.tb01219.x
McFadden PL, McElhinny MW (1988) The combined analysis of remagnetization circles and direct observations in palaeomagnetism. Earth Planets Sci Lett 87(1):161–172. https://doi.org/10.1016/0012-821X(88)90072-6
Miki M (1995) Two-phase opening model for the Okinawa Trough inferred from paleomagnetic study of the Ryukyu arc. J Geophys Res 100(B5):8169–8184. https://doi.org/10.1029/95JB00034
Miyashiro A (1978) Nature of alkalic volcanic rock series. Contrib Mineral Petrol 66(1):91–104. https://doi.org/10.1007/BF00376089
Nakagawa H, Murakai M (1975) Geology of Kumejima, Okinawa Gunto, Ryukyu Islands, Japan. Cont Tohoku Univ Int Geol Pal 75:1–16
Nishimura S, Hashimoto M, Ando M (2004) A rigid block rotation model for the GPS derived velocity field along the Ryukyu arc. Phys Earth Planets Inter 142(3):185–203. https://doi.org/10.1016/j.pepi.2003.12.014
Ogasawara M (1997) K-Ar age and geochemical characteristics of the quartz-porphyry at Shimama, southern Tanegashima, and K-Ar age of a lamprophyre from northern Tanegashima: implications for Miocene igneous activities in the outer zone of Southwest Japan. J Miner Petrol Econ Geol 92(11):454–464. https://doi.org/10.2465/ganko.92.454
Ogg JG (2020) Chapter 5—Geomagnetic polarity time scale. In: Gradstein FM, Ogg JG, Schmitz MD, Ogg GM (eds) Geologic Time Scale 2020. Elsevier, Amsterdam, pp 159–192
Okino K (2015) Magnetic anomalies in the Philippine Sea: implications for regional tectonics. J Geogr 124(5):729–747. https://doi.org/10.5026/jgeography.124.729
Okino K, Ohara Y, Kasuga S, Kato Y (1999) The Philippine Sea: new survey results reveal the structure and the history of the marginal basins. Geophys Res Lett 26(15):2287–2290. https://doi.org/10.1029/1999GL900537
Onoue T, Nagai K, Kamishima A, Seno M, Sano H (2004) Origin of basalts from Sambosan accretionary complex, Shikoku and Kyushu. J Geol Soc Japan 110(4):222–236. https://doi.org/10.5575/geosoc.110.222
Osozawa S, Aita Y, Nakamori T, Niibe A, Kanisawa S, Nakagawa H (1983) Geology of Amami Oshima, central part of the Ryukyu Islands, with special reference to effect of gravity transportation on geologic construction. Mem Geol Soc Japan 22:39–56
Raffi I, Wade BS, Pälike H, Beu AG, Cooper R, Crundwell MP, Krijgsman W, Moore T, Raine I, Sardella R, Vernyhorova YV (2020) Chapter 29—The Neogene Period. In: Gradstein FM, Ogg JG, Schmitz MD, Ogg GM (eds) Geologic time scale 2020. Elsevier, Amsterdam, pp 1141–1215
Saccani E (2015) A new method of discriminating different types of post-Archean ophiolitic basalts and their tectonic significance using Th-Nb and Ce-Dy-Yb systematics. Geosci Front 6(4):481–501. https://doi.org/10.1016/j.gsf.2014.03.006
Safonova I, Kojima S, Nakae S, Romer RL, Seltmann R, Sano H, Onoue T (2015) Oceanic island basalts in accretionary complexes of SW Japan: tectonic and petrogenetic implications. J Asian Earth Sci 113:508–523. https://doi.org/10.1016/j.jseaes.2014.09.015
Sasaki T, Yamazaki T, Ishizuka O (2014) A revised spreading model of the West Philippine Basin. Earth Planets Space 66(1):1–9. https://doi.org/10.1186/1880-5981-66-83
Shinjo R, Kato Y (2000) Geochemical constraints on the origin of bimodal magmatism at the Okinawa trough, an incipient back-Arc basin. Lithos 54(3):117–137. https://doi.org/10.1016/S0024-4937(00)00034-7
Shinjo R, Chung S, Kato Y, Kimura M (1999) Geochemical and Sr-Nd isotopic characteristics of volcanic rocks from the Okinawa Trough and Ryukyu Arc: implications for the evolution of a young, intracontinental back arc

basin. J Geophys Res Solid Earth 104(B5):10591–10608. https://doi.org/10.1029/1999JB900040
Shinjoe H, Orihashi Y, Sumii T (2010) U-Pb zircon ages of syenitic and granitic rocks in the Ashizuri igneous complex southwestern Shikoku: Constraint for the origin of forearc alkaline magmatism. Geochem J 44(4): 275–283. https://doi.org/10.2343/geochemj.1.0070
Shinjoe H, Sumii T, Orihashi Y (2003) Near trench igneous activities in middle Miocene Southwest Japan Arc: connection between magmatism and subduction of hot Shikoku Basin. Month Earth 43:31–38
Sun SS, McDonough WF (1989) Chemical and isotopic systematics of oceanic basalts: implications for mantle composition and processes. Geol Soc London 42(1):313–345. https://doi.org/10.1144/GSL.SP.1989.042.01.19
Taneda S, Kinoshita K (1972) An alkaline rock body in Tanegashima Island, South Kyushu Japan. Bull Volcanol Soc Japan 17(2):88–97. https://doi.org/10.18940/kazanc.17.2_88
Tatsumi Y (2006) High-Mg andesites in the setouchi volcanic belt, Southwestern Japan: analogy to Archean magmatism and continental crust formation? Annu Rev Earth Planets Sci 34(1):467–499. https://doi.org/10.1146/annurev.earth.34.031405.125014
Tatsumi Y, Hanyu T (2003) Geochemical modeling of dehydration and partial melting of subducting lithosphere: toward a comprehensive understanding of high-Mg andesite formation in the Setouchi volcanic belt SW Japan. Geochem Geophys Geosystems 4(9):1081. https://doi.org/10.1029/2003GC000530
Tatsumi Y, Kani T, Ishizuka H, Maruyama S, Nishimura Y (2000) Activation of pacific mantle plumes during the carboniferous; evidence from accretionary complexes in Southwest Japan. Geology 28(7):580–582. https://doi.org/10.1130/0091-7613(2000)28%3c580:AOPMPD%3e2.0.CO;2
Tatsumi Y, Suenaga N, Yoshioka S, Kaneko K, Matsumoto T (2020) Contrasting volcano spacing along SW Japan arc caused by difference in age of subducting lithosphere. Sci Rep 10(1):15005. https://doi.org/10.1038/s41598-020-72173-6
Tauxe L, Kent DV (2004) A Simplified Statistical Model for the Geomagnetic Field and the Detection of Shallow Bias in Paleomagnetic Inclinations: was the Ancient Magnetic Field Dipolar? In: Meert JG, Channell JET, Kent DV et al (eds) Timescales of The Paleomagnetic Field. American Geophysical Union, Washington, DC, pp 101–115
Uto K, Hirai H, Goto K, Arai S (1987) K-Ar ages of carbonate- and mantle nodule-bearing lamprophyre dikes from Shingu, central Shikoku. Southwest Japan Geochem J 21(6):283–290. https://doi.org/10.2343/geochemj.21.283
Wallis SR, Yamaoka K, Mori H, Ishiwatari A, Miyazaki K, Ueda H (2020) The basement geology of Japan from A to Z. Island Arc 29(1):e12339. https://doi.org/10.1111/iar.12339
Zheng Y (2019) Subduction zone geochemistry. Geosci Front 10(4):1223–1254. https://doi.org/10.1016/j.gsf.2019.02.003
Zijderveld JDA (1967) The natural remanent magnetizations of the Exeter volcanic traps (Permian, Europe). Tectonophys 4(2):121–153. https://doi.org/10.1016/0040-1951(67)90048-0
Kato Y (1985) Geology of Tonaki-jima Island. In: Kizaki K (ed) Geology of the Ryukyu Arc Okinawa Times Co., Naha, Japan, p 119–123
Takeuchi M (1993) Geology of the Yuwan district. With Geological Sheet Map at 1: 50,000. Geological Survey of Japan. 69.

Publisher's Note